Targeting G-rich DNA Structures with Photo-Reactive bis-Cyclometalated Iridium(III) Complexes

Justin Weynand, Hugues Bonnet, Frédérique Loiseau, Jean-Luc Ravanat, Jérôme Dejeu, Eric Defrancq, Benjamin Elias

Targeting G-rich DNA Structures with Photo-Reactive bis-Cyclometalated Iridium(III) Complexes

Justin Weynand,[a,b] Hughes Bonnet,[b] Frédérique Loiseau,[b] Jean-Luc Ravanat,[c] Jérôme Dejeu,[b] Eric Defrancq,[*,b] Benjamin Elias[*,a]

[a] *Université catholique de Louvain (UCLouvain), Institut de la Matière Condensée et des Nanosciences (IMCN), Molecular Chemistry, Materials and Catalysis (MOST), Place Louis Pasteur 1, bte L4.01.02, B-1348 Louvain-la-Neuve, Belgium*

[b] *Univ. Grenoble Alpes, CNRS, DCM UMR5250, F-38000 Grenoble, France*

[c] *Univ. Grenoble Alpes, CEA, CNRS, INAC-SyMMES, 17 rue des martyrs, 38054, Grenoble CEDEX 9, France*

ABSTRACT

In this work, we report on the synthesis and the characterisation of three novel iridium(III) bis-cyclometalated complexes. Their photophysics has been fully characterized by classical methods and revealed charge transfer (CT) and ligand centered (LC) transitions. Their ability to selectively interact with G-quadruplex telomeric DNA over duplex DNA has been studied by Circular Dichroïsm (CD), Bio Layer Interferometry (BLI) and Surface Plasmon Resonance (SPR) analyses. Interestingly, one of them is able to perform photo-induced electron transfer (PET) with guanine DNA base, which can in turn lead to oxidative damage (such as 8-oxo-guanine) to the telomeric sequence. To the best of our knowledge, this is the first study of highly photo-oxidant bis-cyclometalated iridium(III) complexes towards G-quadruplex telomeric DNA.

Introduction

The double-helical structure of DNA in which two antiparallel strands are held together through canonical A/T and G/C base pairing was resolved over half a century ago. Beyond canonical double-helical-based structures such as B-DNA, A-DNA, and Z-DNA, the past decades have brought accumulating evidences of the existence and biological relevance of four-stranded nucleic acid motifs. In particular, guanine rich nucleic acids can adopt peculiar secondary structures, globally known as G-quadruplex nucleic acid (**G4-DNA** and **G4-RNA**).[1] They consist in stacked tetrads of Hoogsteen hydrogen-bonded guanine bases, connected by various loop-forming sequences, and are stabilized by physiologically abundant K^+ and Na^+ cations. Sequencing and bioinformatics analyses of the human genome indicate that it contains as much as 700,000 sequences having the potential to form stable G-quadruplex structures.[2, 3] **G4-DNA** forming sequences are found in the promoter regions of a large number of genes, including proto-oncogenes c-MYC, c-KIT, and KRAS as well in viral genome.[4, 5] The most documented biological function of G-quadruplexes concerns certainly telomere homeostasis.[6] Telomeric DNA are guanine rich sequences found in the extremity of the genome. They have critical roles to the cell's life such as protecting the chromosome or being involved in the senescence process.[7, 8, 9] Telomeres of healthy cells progressively decrease after each cell division, until reaching a critical length (Hayflick limit) for which the cells no further divide and enter into senescence. However, in cancer cells, the Hayflick limit is never reached, thus preventing senescence and leading to cell immortality. Two main processes are involved in telomere maintenance; (*i*) the telomerase overexpression which can elongate the telomeric sequence[10] or (*ii*) the alternative lengthening of telomeres (ALT) based on homologous recombination-mechanism.[11]

The stabilization of the G-quadruplexes by small organic molecules,[12] or metal complexes[13] have been the subject of many intense researches over the past decade to design molecules displaying a good

affinity for G4-DNA and selectivity for G-quadruplex *over* duplex DNA. This approach is now considered as useful molecular tool to enhance and/or promote quadruplex related biological effects in cells and shows high potential for future therapies.[14]

In this context, metal complexes show a number of advantages in comparison to organic compounds. They have a net positive charge, a tuneable geometry and many of them show exploitable photochemical properties. At this end, many metal complexes have been designed to stabilize G-quadruplex DNA, in order to prevent the telomerase action. These metal complexes include nickel(II) salphen,[15] platinum(II)[16] and ruthenium(II) polypyridine complexes.[17] Very few metal complexes able to target and photo-damages G-quadruplex DNA have been reported.[18] Recently, Thomas *and coll.* reported the use of a dinuclear ruthenium(II) complex able to photo-oxidize guanosine moieties in duplex and G-quadruplex DNA. [18a] We also reported on new tetraazaphenanthrene (TAP) ruthenium (II) complexes that can selectively interact with G-quadruplex over duplex DNA and are able to perform photo-induced electron transfer (PET) with guanine base.[18b] Interestingly, these complexes described by Thomas *and coll.* and by us showed very interesting photo-cytotoxic effects.

Cyclometalated iridium(III) complexes have been also extensively studied thanks to their photophysical and photochemical properties including high luminescence quantum yields, long excited state lifetimes, large Stoke's shifts and strong photo-stability. Various applications including organic light-emitting diodes (LEDs) design[19] or photocatalytic hydrogen production[20] have been reported. In the context of G-quadruplex DNA, few cyclometalated iridium complexes have been described. Ma *and coll*. have explored a variety of mononuclear iridium(III) complexes as G-quadruplex-selective probes for the construction of a range of label-free luminescent detection platforms.[21]. Sleiman *and coll.* have reported the complex $[Ir(ppy)_2(p\text{-}CPIP)]^+$ **1**, based on 2-(4-chlorophenyl)-1H-imidazo[4,5-f][1,10]phenanthroline (CPIP), for which luminescence studies revealed its high ability to selectively

probe G-quadruplex DNA over duplex DNA.[22] We have recently reported the study of bis-cyclometalated and bis-tridentate iridium complexes with the ability to perform photo-induced electron transfer (PET) with guanine and adenine DNA bases thanks to π-deficient ancillary ligands.[23]

In this context, we thus envisaged to develop new bis-cyclometalated iridium(III) complexes which can interact and photo-react through type I and II photo-oxidation with genetic materials, in particular with telomeric G-quadruplex DNA. In this work, we report on the synthesis and the characterization of three new bis-cyclometalated iridium complexes **2-4** obtained from the coordination of two bis-cyclometalated ligands (ppy = 2-phenylpyridine or 2,2‘-C^N = 1-methyl-[2,2'-bipyridin]-1-ium) and with a diimine ligand (CPIP and CPITAP). CPIP ligand was chosen because it has been reported as an efficient G-quadruplex ligand (*vide supra*) [18b,22] and CPITAP (2-(4-chlorophenyl)-1H-imidazo[4,5-f]pyrazino[2,3-h]quinoxaline) was based on CPIP ligand by modifying the phenanthroline imidazole ligand with the more π-deficient TAP ligand. Complexes based on (2,2’-C^N) ancillary ligands have the advantage of being highly soluble in aqueous solvent thanks to their positive charges.[24] Photophysical properties of compounds **1-4** were investigated and revealed arguments in the favour of mixed charge transfer (CT) and ligand centered (LC) transitions. Interestingly, as evidenced by luminescence spectroscopy, complexes **3-4** are highly oxidant under light irradiation. The affinity and selectivity of complexes **3-4** towards G-quadruplex DNA were studied using CD melting (Tm), Bio Layer Interferometry (BLI) and Surface Plasmon Resonance (SPR).

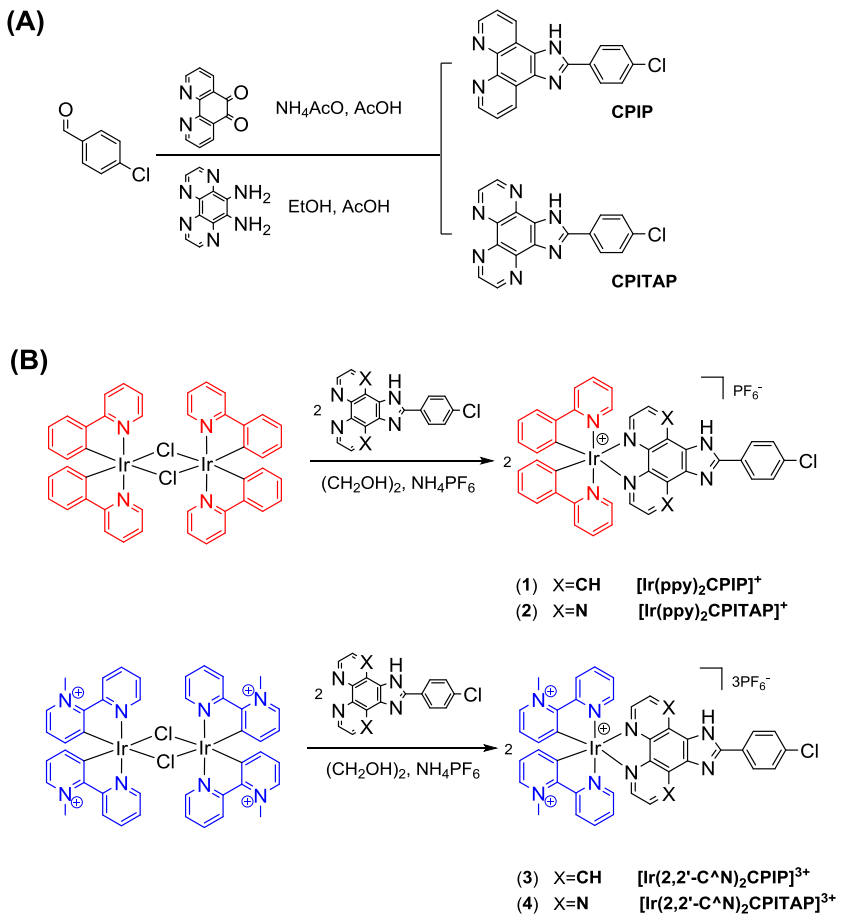

Scheme 1. Synthesis of (A) CPIP- CPITAP ligands and (B) Ir(III) complexes **1-4**.

Results and Discussion

Synthesis of complexes 1-4 (Scheme 1)

The synthesis of CPIP and CPITAP ligands was achieved according to methodologies previously described in the literature. Briefly, CPIP ligand was synthesized by condensation of 4-chlorobenzaldehyde with 1,10-phenanthroline-5,6-dione in an ammonium medium.[22] CPITAP ligand was obtained through the reaction of 4-chlorobenzaldehyde and 9,10-diamino-1,4,5,8-tetraazaphenanthrene in a refluxing acetic acid/ethanol mixture.[18b] The corresponding Ir(III) complexes **1-4** were prepared by direct chelation of the N^N ligand (CPIP or CPITAP) onto a Ir(III) precursor bearing either phenylpyridine $[Ir(ppy)_2Cl]_2$ or *N*-methylphenylpyridine $[Ir(2,2'\text{-}C\text{^}N)_2Cl]_2$ ligand.

Complexes **1-4** were purified over preparative SiO_2 chromatography to afford the hexafluorophosphate salts pure final compounds. They have been unambiguously characterized by ^1H NMR spectroscopy and high-resolution mass spectrometry (see the Experimental Section and Figures S1-S6 and S7-S9) as well as by UV-vis, cyclic voltammetry (CV) and photochemical studies (*vide infra*).

Absorption and Luminescence Properties

The photophysical properties of complexes **1-4** were assessed in acetonitrile and water. The absorption spectra of complexes **1-4** in acetonitrile at 298 K are shown in Figure 1 and in the supporting information (see Figures S10-S11). The corresponding spectroscopic data are summarized in Table **1**. All complexes display intense absorption bands in the UV area (250 to 300 nm) with high molar extinction coefficients ($\varepsilon > 20\ 000\ M^{-1}cm^{-1}$). By comparison with literature and absorption spectra of free ligand in solution, these bands are assigned to ligand centered (LC) transitions. At lower energy ($\lambda > 340$ nm), charge transfer (CT) transitions can be observed with lower molar extinction coefficients ($\varepsilon < 20\ 000\ M^{-1}cm^{-1}$).

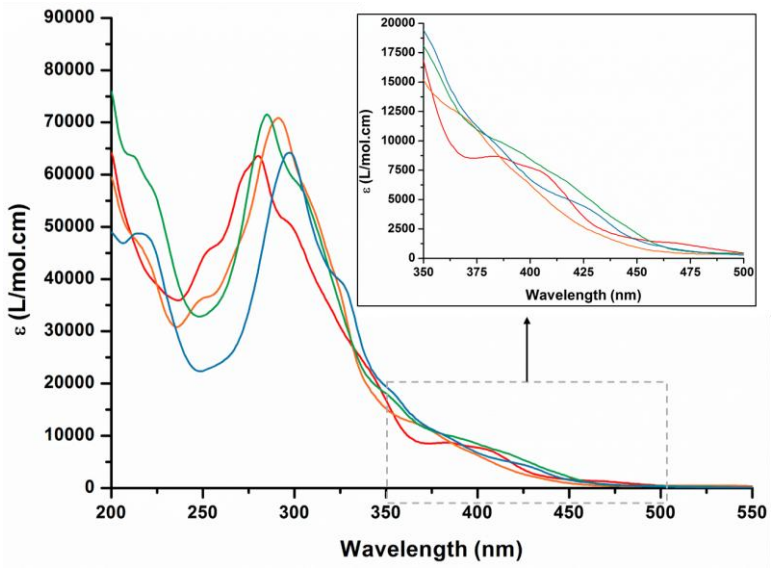

Figure 1. UV-vis absorption spectra of complexes **1** (red), **2** (orange), **3** (green) and **4** (blue), recorded in

acetonitrile at 298 K. Inset: zoom of the 350-500 nm region.

The emission spectra for complexes **1**-**4** were recorded in deoxygenated and oxygenated acetonitrile or water. The luminescence data are gathered in Table **1** (see Figures S10-S13).

Table 1. Absorption and luminescence data for complexes **1**-**4**.

	λ_{Abs} (ε) [a]	λ_{Em} [b]			Φ_{Em} [c]		τ (ns) [d]	
Complex	CH_3CN	CH_3CN	H_2O	77K	CH_3CN	H_2O	CH_3CN	H_2O
1	453	583	*n.d.*	536	0.036	*n.d.*	67	*n.d.*
	(1.56)				(0.15)	*n.d.*	(441)	*n.d.*
2	400	697	*n.d.*	615	$<1.10^{-3}$	*n.d.*	14	*n.d.*
	(6.27)				$<1.10^{-3}$	*n.d.*	(12)	*n.d.*
3	417	528	528	504, 544	0.067	0.0018	613	316
	(6.40)				(0.136)	(0.0018)	(950)	(560)
4	429	528	528	504, 544	$<1.10^{-3}$	$<1.10^{-3}$	6	7
	(4.04)				(0.001)	$<1.10^{-3}$	(9)	(8)

[a] λ in nm for the most bathochromic absorption in MeCN (extinction coefficient, ε x 10^3 $M^{-1}cm^{-1}$). [b] λ in nm at RT in MeCN, H_2O and at 77K in EtOH/MeOH (4/1, v/v). [c] Quantum yield of emission measured by comparison with the reference $[Ru(bpy)_3]^{2+}$, under air and under argon (in brackets), excitation at 450 nm, errors are estimated to 10%. [d] Luminescence lifetime (after irradiation at λ = 400 nm) measured under air and under argon (in brackets), errors are estimated to 5%. *n.d.*: not determined due to the very low solubility of the chloride salt in water.

Complex **1** exhibited luminescence in the orange area of the visible spectrum, consistent with literature data.[22] The bathochromic emission shift from **1** to **2** can be explained by the stabilized LUMO of the electron-deficient ligand CPITAP.

The emission spectra of complexes **1** and **2** at 77K are blue shifted compared to organic solvent (Table 1), providing some evidence for a charge transfer (CT) character of the excited state. According to Coe *et coll.*, the radiative process for Ir(III) complexes bearing C^N bpy-Me ligands (such as **3**-**4**) is ascribed to a mixture of ^{3}LC and ^{3}MLCT.[25] It is therefore reasonable to assume that the same manifold of excited states is operative in our compounds, i.e. complexes **3**-**4** should possess predominant ^{3}LC (π (2,2'-C^N) to π* (2,2'-C^N)) and ^{3}MLCT (dπ (Ir) to π* (2,2'-C^N)) characters.[25]

For all complexes **1**-**4**, the quantum yield of emission (Φ) and luminescence lifetime (τ) measured in acetonitrile increased from air to argon, suggesting their ability to photosensitize triplet oxygen into singlet oxygen. The low quantum yields for complex **4** in both organic and aqueous solvent and for complex **2** in organic solvent could be explained by the increase of non-radiative process due to interaction of the solvent with non-chelating nitrogen atoms of CPITAP ligand. As the solubility of complexes **1**-**2** was very low in aqueous solvent, no quantum yield and luminescence data could be obtained in water.

Electrochemical Study

The redox properties of **1**-**4** were investigated by cyclic voltammetry experiments in dry deoxygenated acetonitrile, the data are gathered in Table **2** (see also Figures S14-S17).

Complexes **1**-**2** displayed a one-electron reversible oxidation wave, usually attributed to the oxidation of the Ir-phenylpyridine moiety.[22] For complexes **3**-**4**, no oxidation could be detected below 2 V *vs* Ag/AgCl, likely due to the presence of the pyridinium unit on the cyclometalated ligands stabilizing the HOMO orbital of the complex. This is consistent with the oxidation data of similar complexes already published.[25] Indeed, Coe *et coll.* described one irreversible oxidation for similar compounds in the region *ca.* 2.2-2.5 V, which was assigned to the Ir^{IV}/Ir^{III} couple. For the reduction, the wave observed for complex **1** corresponds to the reduction of the phen moiety of the CPIP ligand.[22] The anodic shift

from **1** to **2** is consistent with the higher π-deficiency of the TAP moiety of CPITAP ligand as previously described.[18b] Finally, the reduction waves observed for complexes **3**-**4** correspond to the multiple reduction of the pyridinium unit.[25] From the cyclic voltammetry measurements and the spectroscopic data, the oxidation and the reduction potential at the excited state can be roughly estimated. From the analysis of these values, the complexes **3** and **4** display a much higher photo-oxidizing power (+1.59 V *vs* Ag/AgCl) compared to complexes **1**-**2**.

Table 2. Electrochemical data of complexes **1**-**4.**

Complex	$E_{ox\ 1/2}$	$E^*_{ox}{}^a$	$E_{red\ 1/2}$	$E^*_{red}{}^a$
1	+ 1.35	-0.78	-1.57	0.56
2	+ 1.38	-0.40	-0.72	1.06
3	> 2	*	-0.76	1.59
4	> 2	*	-0.76	1.59

Data were measured at room temperature in deoxygenated MeCN with 0.1M Bu_4NClO_4 as the supporting electrolyte (V *vs* Ag/AgCl reference electrode), complex concentration = 0.8 mM, [a] Excited state potentials estimated from equations $E^*_{ox} = E_{½\ ox} - E_{0-0}$ and $E^*_{red} = E_{½\ red} + E_{0-0}$. The energy of the excited state, $E_{0\text{-}0}$, was assimilated to the maximum of the emission spectrum in acetonitrile at 298 K. * could not be estimated due to impossibility to measure E_{ox} of the ground state.

Study of the interaction with telomeric G-quadruplex and duplex DNA

A number of biophysical techniques including optical and fluorescence spectroscopy, melting temperature measurements, CD spectroscopy, Isothermal Titration calorimetry (ITC) and Surface Plasmon Resonance (SPR) have been developed to study the interactions of ligands with G-quadruplex DNA.[26] In the present study, we have performed CD melting temperature measurements (Tm), Bio Layer Interferometry (BLI) and Surface Plasmon Resonance (SPR) studies. Due to the very low

solubility of complexes **1**-**2** in water, we have conducted the studies only with complexes **3**-**4**.

CD spectroscopy and melting assays (Tm)

First, the ability of complexes **3-4** to interact with DNA was investigated by CD experiments with both duplex ($^{5'}CGT_3CGT_5ACGA_3CG^{3'}$ hairpin) and G-quadruplex (wtTel23, $^{5'}TAGGG(TTAGGG)_3{}^{3'}$) DNA. The study was carried out in 100 mM NaCl or 100 mM KCl buffer (10 mM Tris-HCl, pH 7.04). As mentioned in the introduction, the choice of the cation highly influences the structure of the G-quadruplex. In sodium buffer, wtTel23 folded into an antiparallel topology characterized by two positive peaks at 242 nm and 294 nm, and a negative peak at 262 nm, whereas in potassium buffer, a maximum was observed at 290 nm with a shoulder at 270 nm, corresponding to the hybrid II-type G4. Hairpin duplex DNA was characterized by a negative peak at 251 nm. Upon addition of complexes **3-4** in sodium containing buffer, no change in the CD spectra of wtTel23 and duplex DNA were observed whereas minor changes in the ellipticity of wtTel23 were observed for complex **3** in potassium buffer. Nevertheless, these results suggested that the complexes did not induce major structural changes in the conformation of G-quadruplex and duplex DNA (see Figures S18-S20). We then performed CD melting assays to assess the thermal stabilization induced by the interactions of the complexes with wtTel23 and duplex DNA (Figure **2** and Figures S21-S23).

CD melting curves of wtTel23 and GC rich hairpin duplex have been recorded in the absence or the presence of each complex (at 5:1 complex/DNA ratio). CD melting experiments results clearly showed that complexes **3-4** did not significantly alter the stability of the hairpin duplex whereas a slight stabilization of wtTel23 with complex **3** was observed in both sodium and potassium buffer. However, it should be noticed that for studies in potassium containing buffer, the measurement is quite more arduous due to a slight change in the conformation of wtTel23. This was confirmed by observing the CD spectra at different temperatures (Figure S22). Surprisingly, complex **4** did not stabilize the

telomeric sequence, in both buffers. This observation has already been described previously with the same ligand CPITAP.[18b] With these results in hand, we continued with more appropriate methods that allowed us to measure kinetic (k_{on}-k_{off}) and thermodynamic values (K_D).

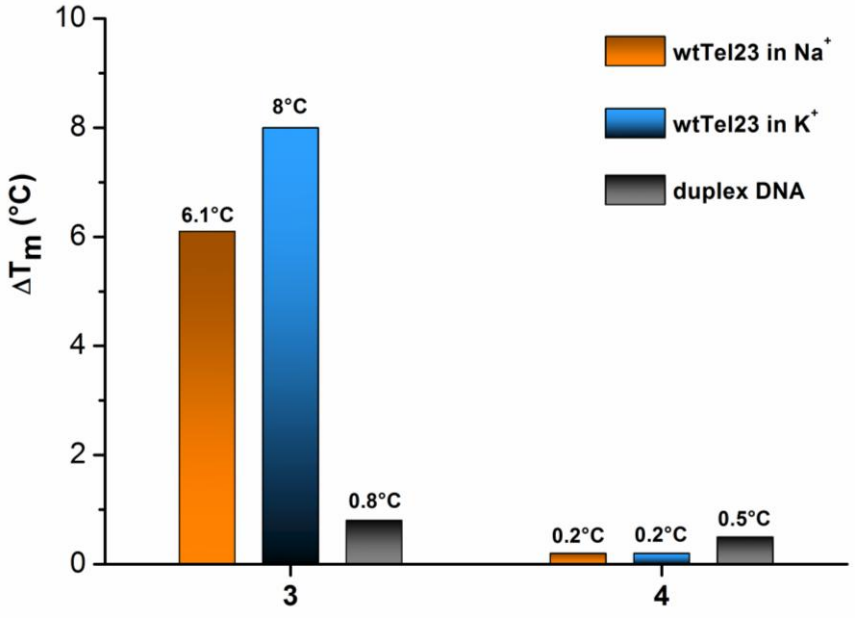

Figure 2. Variation of melting temperatures (ΔT_m) of wtTel23 and duplex hairpin measured between the absence and the presence of complexes **3**-**4**. WtTel23 $^{3'}$TT(GGGATT)$_3$GGG$^{5'}$ and hairpin $^{5'}$CGT$_3$CGT$_5$ACGA$_3$CG$^{3'}$ sequences were first annealed by heating at 95°C for 5 min in Tris-HCl buffer (10 mM, pH 7.04) with 100 mM NaCl or 100 mM KCl (only for wtTel23) and cooled down overnight to room temperature, then complex **3** or **4** (5 equiv.) was added.

Bio Layer Interferometry (BLI) and Surface Plasmon Resonance (SPR) studies

In order to determine the thermodynamic and kinetic parameters of the interaction, we employed Bio Layer Interferometry (BLI) and Surface Plasmon Resonance (SPR) methods. These methods have been used previously in our group to study the interaction of ruthenium(II) complexes with different G-quadruplex structures.[17b, 18b] In the present study, we performed BLI experiments with both complexes **3**-**4**. For this aim, the following systems were used: the intramolecular G-quadruplex **A** (HTelo sequence

in equilibrium between different topologies), the human telomeric sequence (HTelo) constrained in a single antiparallel topology **B** and hairpin DNA **C**. System **B** allows the precise control of G-quadruplex topology (in this case antiparallel) through assembly of constrained structures on a template.[27]

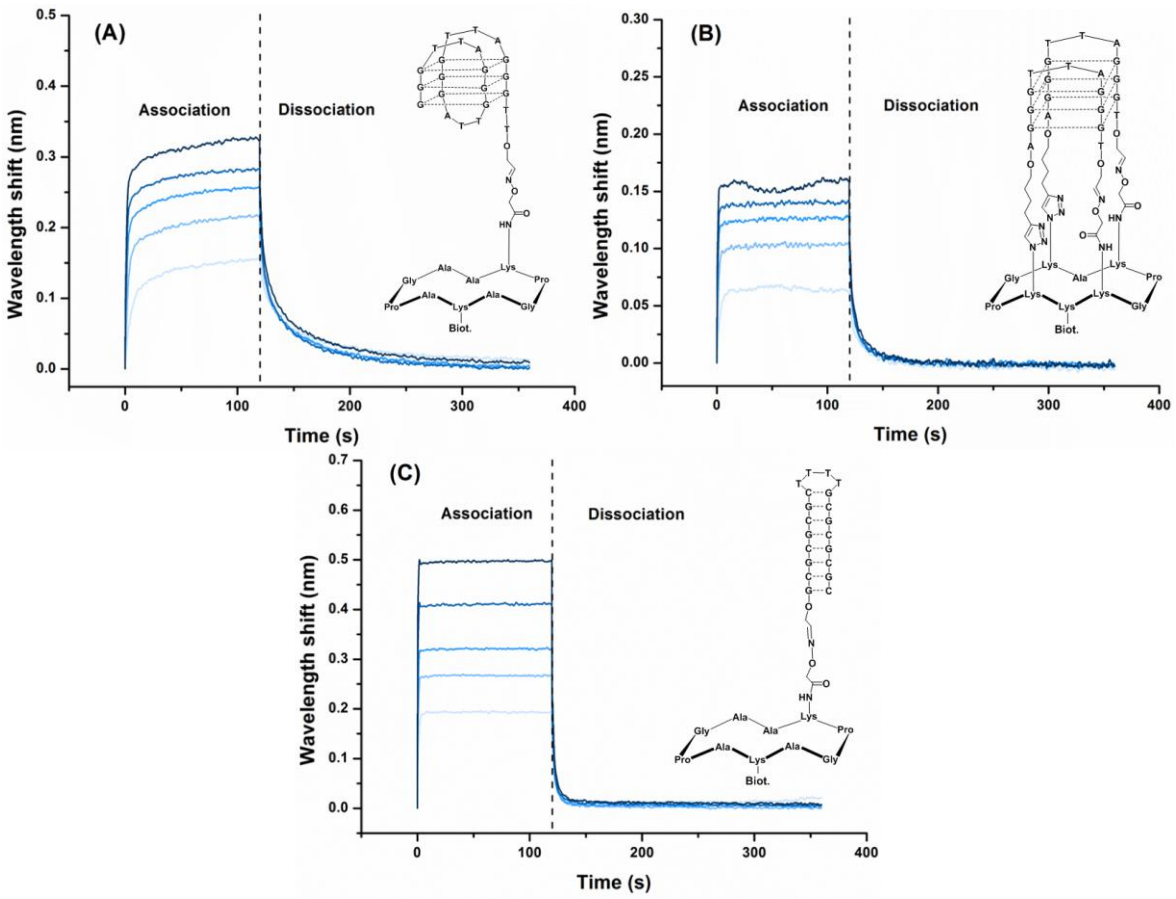

Figure 3. BLI sensorgrams of complex **3** in interaction with G-quadruplex systems **A**-**B** and duplex control **C**. (**A**) intramolecular like G-quadruplex; (**B**) human telomeric sequence constrained in an antiparallel topology and (**C**) duplex (hairpin). The running buffer were 10 mM HEPES (10 mM, pH 7.4) with 35 mM NaCl, 50 mM KCl and 0.5% v/v surfactant.

The two complexes **3** and **4** showed K_D values in the micromolar range for G-quadruplex structures **A** and **B** (Table 3 and Figure S24). These values fall within the range of those reported for similar ruthenium(II) complexes interacting with G-quadruplexes. It is noteworthy that the affinity of complex

3 towards G-quadruplex DNA is significantly higher than that of complex **4** (Table **3** and see Figure S24). This is in agreement with the melting temperature (*Tm*) study (*vide supra*). However, a weak selectivity for G-quadruplex structure *versus* duplex DNA was obtained. This could be explained by the net positive charge of Ir(III) complexes in comparison to Ru(II) complexes that could favour non-specific ionic interactions with the DNA phosphodiester backbone. This is also in agreement with the low ΔTm obtained from CD melting analysis.

Table 3. Interaction of complexes **3** and **4** with quadruplex **A** and **B**, and duplex **C** DNA structures, determined by BLI experiments.

	Quadruplex system **A**			Quadruplex system **B**			Duplex system **C**		
	k_{on} (10^4 M^{-1} s^{-1})	k_{off} (10^{-1} s^{-1})	K_D[a] **(μM)**	k_{on} (10^4 M^{-1} s^{-1})	k_{off} (10^{-1} s^{-1})	K_D[a] **(μM)**	k_{on} (10^4 M^{-1} s^{-1})	k_{off} (10^{-1} s^{-1})	K_D[a] **(μM)**
3	*9 ± 2*	*4 ± 1*	**4 ± 1**	*19 ± 2*	*6 ± 2*	**3 ± 1**	*5 ± 1*	*17 ± 2*	**34 ± 7**
4	*3 ± 1*	*13 ± 1*	**46 ± 14**	*3 ± 1*	*18 ± 2*	**56 ± 7**	*1 ±1*	*14 ± 1*	**120 ± 1**

[a] Equilibrium dissociation constants deduced from the kinetic rate constants. The errors provided are standard deviations from the mean values. The running buffer were 10 mM HEPES (10 mM, pH 7.4) with 35 mM NaCl, 50 mM KCl and 0.5% v/v surfactant.

To confirm the data obtained from BLI measurements, Surface Plasmon Resonance (SPR) analysis was performed with the most promising complex **3** (Figure S25 and Table S1). For G-quadruplex structure **A** and **B**, we obtained a dissociation constant (K_D) of 4 and 2 μM, respectively. For the duplex hairpin system **C**, a dissociation constant of 28 μM was determined. As anticipated, the values are very close from the ones obtained from BLI experiments.

For complex **3**, the kinetic data (k_{on} and k_{off} values, Table 3) were also compared with previously reported similar ruthenium complexes $[Ru(phen)_2CPIP]^{2+}$ (**Ru-1**) and $[Ru(TAP)_2CPIP]^{2+}$ (**Ru-3**) and well-known G4 ligands (PhenDC3, Braco-19 and TMPyP4).[18b, 28] As illustrated in Figure **4**, complex **3** shows association and dissociation rates similar to those of TMPyP4 and $[Ru(TAP)_2CPIP]^{2+}$.

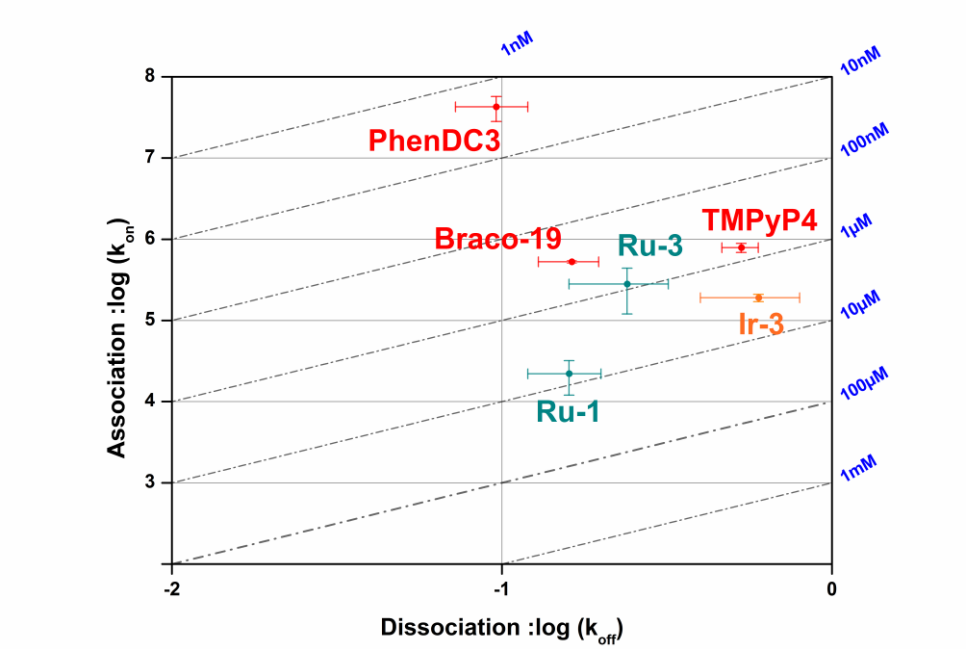

Figure 4. Isoaffinity plot and kinetic characterization for G-quadruplex structure **B**. For PhenDC3, Braco-19 and TMPyP4 (in red) the analyses were performed by SPR[28], for ruthenium(II) complexes (in turquoise) [18b] and iridium(III) complex **3** (in orange) from BLI analysis. K_D (parallel diagonal lines), k_{on} (association kinetic constant, y-axis), k_{off} (dissociation kinetic constant, x-axis).

Guanine's photo-oxidative damage studies

As G-quadruplex DNA are guanine rich sequences, we investigated the ability of complex **3** to trigger photo-induced electron transfer (PET) with dGMP. This PET is well known to lead to oxidative lesions on DNA.[29] Based on the electrochemical data, complex **3** displays a strong photo-oxidizing ability (1.59 V *vs* Ag/AgCl) towards guanine (E_{ox} = 1.10 V *vs* Ag/AgCl).

Luminescence Quenching Studies in the presence of dGMP and ODNs

First, the ability of complex **3** to photo-abstract an electron from a guanine has been investigated by luminescence quenching experiment. Figure **5** shows the relative emission decrease of complex **3** upon addition of increased concentrations of 2'-deoxyguanosine-5'-monophosphate (dGMP). A linear Stern-Volmer relationship is obtained from these data (inset Figure 5), suggesting a pure dynamic quenching of the excited state of complex **3** in the presence of dGMP. Considering the oxidation power of the excited state of complex **3** and using the empirical Rehm-Weller equation, it is expected that process (**1**) with dGMP will be exergonic respectively by about 0.55 eV. Based on these thermodynamic considerations, we can safely ascribe this luminescence quenching to a photo-induced electron-transfer (PET) process from the guanine unit to the excited state complex (eq **1**).

$$[IrN_4C_2]^{3+}* + G \rightarrow [IrN_4C_2]^{2+} + G^{\bullet+} \qquad (\mathbf{1})$$

The efficient quenching in the presence of guanine units is also in agreement with the high value of the quenching rate constant (2.26×10^9 M^{-1} cm^{-1}) obtained from the Stern-Volmer plot of complex **3** with dGMP close to the diffusion limit.

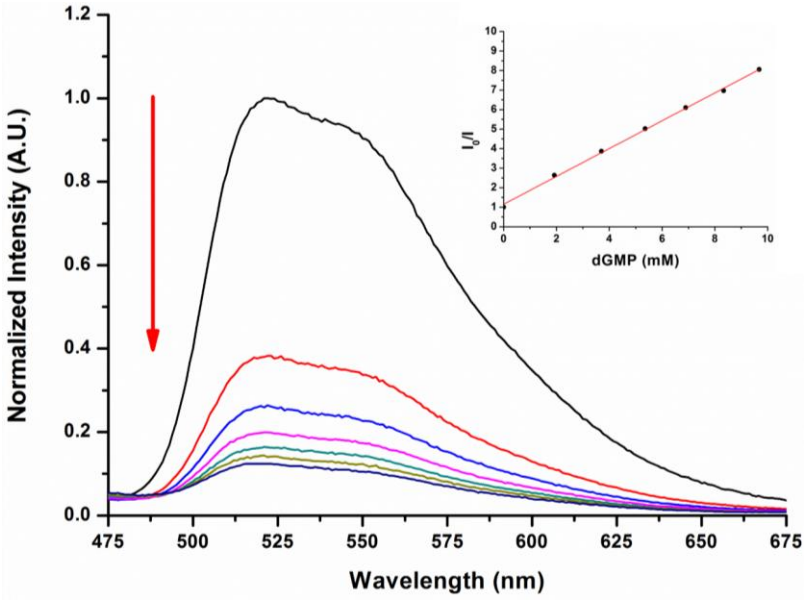

Figure 5. Luminescence titration of complex **3** by dGMP. Experiment carried out in 50 mM TRIS (pH=7.4) aqueous buffer. Excitation was performed at λ = 350 nm. Inset: Stern-Volmer plots obtained upon the addition of dGMP (0 to 10 mM) to **3**.

We further tested whether this PET occurs with guanine embedded into an oligonucleotide sequence. We employed the wtTel23 telomeric sequence, which can fold in G-quadruplex DNA in the presence of a buffer 10 mM HEPES, 35 mM NaCl and 50 mM KCl (pH = 7.4). Figure **6-A** displays the absorption and emission spectra upon addition of increasing concentrations of the telomeric sequence (*i.e.* wtTel23, $^{5'}$TAGGG(TTAGGG)$_3$$^{3'}$). Only weak changes in the absorption spectrum are observed, as already described for similar metal complexes with DNA. The luminescence extinction of **3** was monitored by steady-state fluorescence (Figure **6-B**). The luminescence of **3** was drastically quenched upon addition of wtTel23. In good agreement with the experiment with dGMP (*vide infra*), this luminescence quenching suggests a photo-induced electron transfer (PET) from the guanine-quartet DNA structure. As this electron transfer (ET) can lead to the formation of oxidized guanine (*i.e.* 8-oxo-dG), we further tried to evidence such oxidation products.[29] Control experiment has been performed with a G-rich

duplex DNA (*i.e.* HP GC, $^{3'}(GC)_4TTTT(GC)_4{}^{5'}$), and show a lower quenching efficiency (Figure S26). This suggests a different and better interaction mode with G-quadruplex DNA.

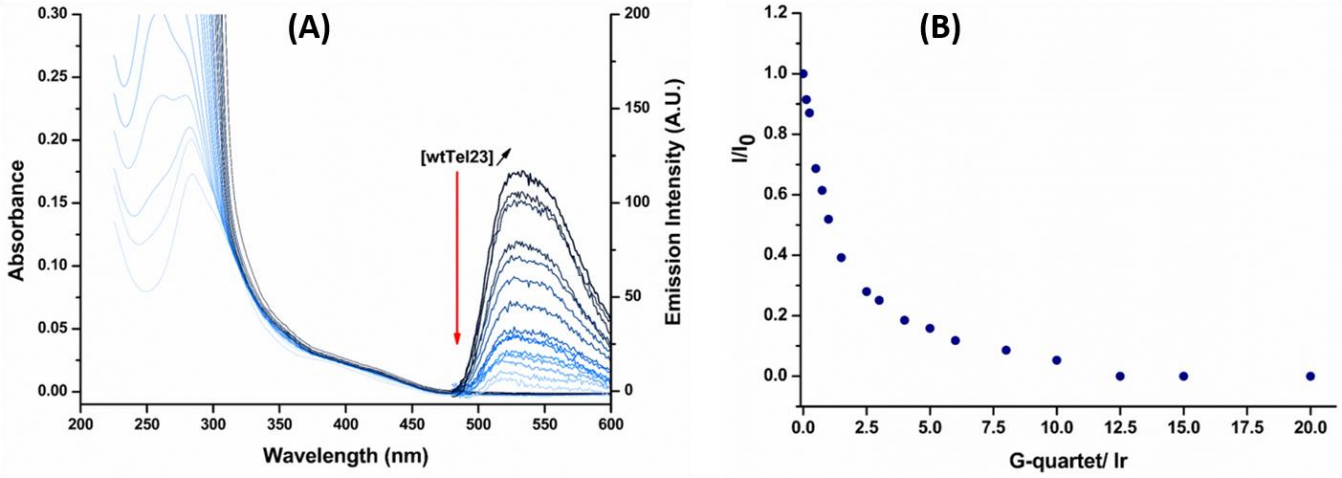

Figure 6. Luminescence titration of complex **3** by the telomeric sequence wtTel23. (**A**) Absorption and emission spectra upon addition of increasing concentration of wtTel23 (**B**) Luminescence titration of **3** by increasing amount of G-quadruplex DNA (wtTel23, G-quartet equivalents per Ir complex), carried out in 10 mM HEPES (pH=7.4), 35 mM NaCl, 50 mM KCl buffer. Excitation was performed at λ = 350 nm.

Photo-Induced Formation of 8-oxodG in the Telomeric Sequence

It is well known in the literature that oxidizing DNA base pairs can lead to the formation of lesions in the genome.[29] In the present study, we were interested in monitoring the formation of the most common product obtained from guanine oxidation, i.e. 8-oxo-7,8-dihydro-2'-deoxyguanosine (8-oxodG). The impact of the formation of 8-oxodG on the G-quadruplex structure from telomeric sequence have been recently studied: depending on the position of 8-oxodG in the telomeric sequence, minor or major structural changes can occur.[30] In this context, the development of compounds that can photo-induce the formation of 8-oxodG in telomeres is of great interest. We have tested whether the most promising complex **3** is able to increase by PET the prevalence of 8-oxodG in the telomeric sequence wtTel23 (Figure **7**).

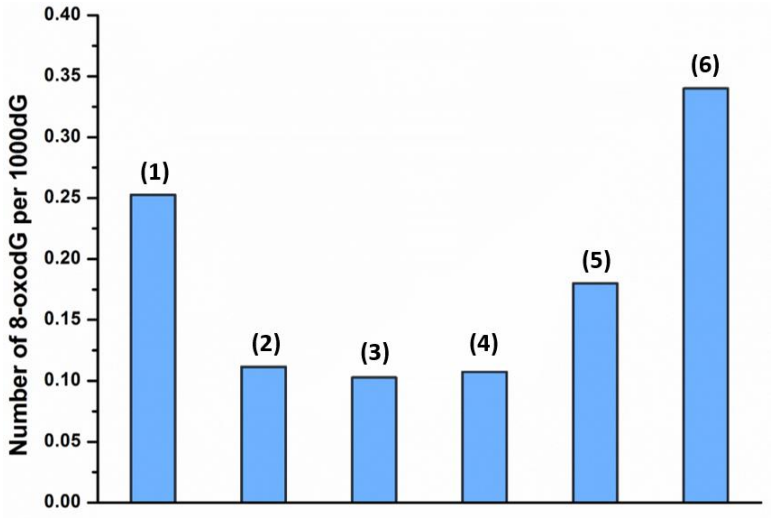

Figure 7. Amount of 8-oxodG/1000 dG formed in the telomeric sequence wtTel23 after (1) addition of complex **3** and 30 min irradiation, (2) addition of **3** without irradiation (3) irradiation of wtTel23, (4) wtTel23 in the dark, (5) addition of $[Ru(bpy)_3]^{2+}$ and 30 min irradiation, and (6) control experiment: complex **3** irradiated 30 min in the presence of the GC rich duplex hairpin (HP-GC). The photoreactions were performed in 10 mM HEPES (pH=7.4), 35 mM NaCl, 50 mM KCl buffer.

The experiment has been performed in comparison with $[Ru(bpy)_3]^{2+}$ complex, which is well-known to induce 8-oxo-dG by type II photo-oxidation (singlet oxygen photo-sensitization).[31] The presence of 8-oxo-dG upon irradiation with iridium complex **3** was shown and demonstrated its ability to photo-react with DNA and generate $G^{\bullet+}$. Moreover, the amount of 8-oxo-dG formed upon irradiation with complex **3** was found to be slightly higher than that with $[Ru(bpy)_3]^{2+}$. Nevertheless, a control experiment with G-rich duplex DNA also shown the formation of 8-oxo-dG with quite the same amount as for telomeric sequence. These results emphasize the ability of iridium complex **3** to induce oxidative photo-lesions in the human genome, even in the structured telomeric sequence.

Conclusion

A series of three new iridium(III) cyclometalated complexes have been designed and synthesized to

target and photo-react with telomeric G-quadruplex DNA. Firstly, the study of their photophysical properties showed a mixture of transitions for all complexes. Interestingly, complex **3** displayed good affinity towards telomeric G-quadruplex DNA and a slight selectivity versus duplex DNA. Thanks to its oxidizing power at the excited state, it is able to photo-react with DNA, likely through a photo-induced charged transfer (PET) with guanine moieties. To the best of our knowledge, this would be one of the first example of iridium(III) complex that can interact with G-quadruplex DNA and trigger electron transfer with guanine under light irradiation. This photo-induced electron transfer (PET) leads to the formation of 8-oxo-dG in the telomeric sequence. Nevertheless, no selectivity of this photo-damage formation was observed for G-quadruplex versus duplex DNA. This could be due to a too low difference of affinity for G-quadruplex versus duplex DNA. Further efforts have thus to be made to improve the affinity for the G-quadruplex target versus duplex DNA to obtain photo-reactive iridium complexes able to selectively target and photo-damage the telomeres of cancer cells.

Experimental Section

Material and methods

$[Ir(ppy)_2Cl]_2$,[32] $[Ir(2,2'\text{-}C\text{^}N)_2Cl]_2$,[25] CPIP,[22] CPITAP [18b] and $[Ir(ppy)_2CPIP]^+$ **1** [22] were synthesized according to previously described literature protocols. All solvents and reagents for the synthesis were of reagent grade and were used without any further purification. All solvents for the spectroscopic and electrochemical measurements were of spectroscopic grade. Water was purified with a Millipore Milli-Q system. ^1H experiments were performed in CD_3CN on a Bruker AM-500 (500 MHz) at 20°C. The chemical shifts (given in ppm) are measured *vs* the residual peak of the solvent as the internal standard. High-resolution mass spectrometry (HRMS) spectra were recorded on a Q-Extractive orbitrap from ThermoFisher using reserpine as internal standard. Samples were ionized by electrospray ioniza-

tion (ESI; capillary temperature = 320°C, vaporizer temperature = 320°C, sheath gas flow rate = 5 mL/min). The studies in acetonitrile and water were performed with the PF_6^- and Cl^- salt, respectively.

Synthesis

[Ir(ppy)$_2$CPITAP].1PF$_6$ 2. $[Ir(ppy)_2Cl]_2$ (20 mg, 0.02 mmol) and CPITAP (13.6 mg, 0.04 mmol) were dissolved in ethylene glycol (2 mL) and heated at 170°C overnight in the dark and under argon. After cooling and addition of aqueous solution of NH_4PF_6, a solid was formed. The latter was washed 3 times with water, EtOH and Et_2O to afford the crude product. Purification over preparative SiO_2 chromatography ($CH_3CN/H_2O/NH_4Cl$(sat) 4/4/1, v/v/v) and addition of NH_4PF_6 gave the final product as a red powder (20 mg, 51%). ^{1}H NMR (500 MHz, CD_3CN): δ = 9.14 (s, 2H), 8.26 (m, 4H), 8.07 (d, 2H, J=8.0 Hz), 7.86 (dd, 2H, J=7.9 Hz, J=0.96 Hz), 7.81 (td, 2H, J=7.6 Hz, J=1.5 Hz), 7.63 (d, 2H, J=11 Hz), 7.53 (d, 2H, J=3.5 Hz), 7.12 (td, 2H, J=7.5 Hz, J=1.2 Hz), 7.01 (td, 2H, J=7.5 Hz, J=1.4 Hz), 6.88 (t, 2H, J=7.2 Hz), 6.34 ppm (dd, 2H, J=7.5 Hz, J=0.7 Hz). HR-MS Calcd for $C_{39}H_{25}N_8ClIr$ (**2** - 1PF_6): 833.151446 Da, found 833.150254 Da.

[Ir(2,2'-C^N)$_2$CPIP].3PF$_6$ 3. $[Ir(2,2'\text{-}C\text{^}N)_2Cl]_2$ (15 mg, 0.009 mmol) and CPIP (6.3 mg, 0.02 mmol) were dissolved in ethylene glycol (2 mL) and heated at 170°C for 48h in the dark and under argon. After cooling and addition of aqueous solution of NH_4PF_6, a solid was formed. The latter was washed 3 times with water, EtOH and Et_2O to afford the crude product. Purification over preparative SiO_2 chromatography ($CH_3CN/H_2O/KNO_3$(sat) 7/0.5/1, v/v/v) and addition of NH_4PF_6 gave the final product as a yellow powder (12 mg, 53%). ^{1}H NMR (500 MHz, CD_3CN): δ = 9.29 (s, 2H), 8.63-8.59 (d, 2H, J=8.5 Hz), 8.49-8.46 (d, 2H, J=6 Hz), 8.38-8.34 (d, 2H, J=8.5 Hz), 8.24 (m, 2H), 8.12 (t, 2H, J=8.7 Hz), 8.01-7.91 (m, 2H), 7.81-7.73 (m, 2H), 7.67-7.64 (d, 2H, J=8.5 Hz), 7.46-7.41 (dd, 2H, J=7.7 Hz, J=6.08 Hz), 7.34-7.30 (d, 2H, J=7.7 Hz), 7.28 (t, 2H, J=13.6 Hz, J=6.2 Hz), 4.71-4.67 ppm (s, 6H). HR-MS Calcd for $C_{41}H_{31}N_8ClF_{12}IrP_2$ (**3** - 1PF_6): 1151.12442 Da, found 1151.12512 Da.

[Ir(2,2'-C^N)$_2$CPITAP].3PF$_6$ 4. [Ir(2,2'-C^N)$_2$Cl]$_2$ (15 mg, 0.009 mmol) and CPITAP (6.3 mg, 0.02 mmol) were dissolved in ethylene glycol (2 mL) and heated at 170°C for 72h in the dark and under argon. After cooling and addition of aqueous solution of NH_4PF_6, a solid was formed. The latter was washed 3 times with water, EtOH and Et_2O to afford the crude product. Purification over preparative SiO_2 chromatography ($CH_3CN/H_2O/KNO_3$(sat) 6/2/2, v/v/v) and addition of NH_4PF_6 gave the final product as a yellow powder (10 mg, 44%). ^{1}H NMR (500 MHz, CD_3CN): δ = 9.29 (s, 2H), 8.64-8.59 (d, 2H, J=8.5 Hz), 8.52-8.47 (d, 2H, J=5.3 Hz), 8.35 (d, 2H, J=8.6 Hz), 8.31-8.26 (d, 2H, J= 2.6 Hz), 8.19-8.13 (t, 2H, J=9 Hz), 7.81 (dd, 2H, J=5.6 Hz, J=0.9 Hz), 7.72-7.65 (d, 2H, J=8.6 Hz), 7.48-7.31 (dd, 2H, J=7.7 Hz, J=6.1 Hz), 7.34-7.28 (t, 2H, J=5.7 Hz), 7.25 (dd, 2H, J=7.7 Hz, J=0.8 Hz), 4.69 ppm (s, 6H). HR-MS Calcd for $C_{39}H_{29}N_{10}ClF_{12}IrP_2$ (**4** - 1PF$_6$): 1153.11492 Da, found 1153.11550 Da.

Absorption and luminescence studies

UV-vis absorption spectra were recorded on a Shimadzu UV-1700. The concentration of the complexes was 10 μM. Room temperature luminescence spectra were recorded on a Varian Cary Eclipse instrument. Luminescence intensity at 77 K was recorded on a FluoroLog3 FL3-22 from Jobin Yvon equipped with an 18 V 450 W Xenon Short Arc lamp and an R928P photomultiplier, using an Oxford Instrument Optistat DN nitrogen cryostat controlled by an Oxford Intelligent Temperature Controller (ITC503S) instrument. Quantum yield were obtained using $[Ru(bpy)_3]^{2+}$ as a reference.[33] Luminescence lifetime measurements were performed after irradiation at λ = 400 nm obtained by the second harmonic of a Titanium:Sapphire laser (picosecond Tsunami laser spectra physics 3950-M1BB+39868-03 pulse picker doubler) at a 8 MHz or 80 kHz repetition rate. The Fluotime 200 from AMS technologies was used for the decay acquisition. It consists of a GaAs microchannel plate photomultiplier tube (Hamamatsu model R3809U-50) followed by a time-correlated single photon counting system from Picoquant (PicoHarp300). The ultimate time resolution of the system is close to

30 ps. Luminescence decays were analysed with FLUOFIT software available from Picoquant.

Electrochemical studies

Cyclic voltammetry was carried out in a one-compartment cell, using a glassy carbon disk working electrode (approximate area = 0.03 cm^2), a platinum wire counter electrode, and an Ag/AgCl reference electrode. The potential of the working electrode is controlled by an Autolab PGSTAT 100 potentiostat through a PC interface. The cyclic voltammograms were recorded with a sweep rate of 100 mV s^{-1}, in dried acetonitrile (Sigma-Aldrich, HPLC grade). The concentration of the complexes was 8.10^{-4} mol/L, with 0.1 mol/L tetrabutylammonium perchlorate as supporting electrolyte. Before each measurement, the samples were purged by nitrogen. Redox potentials were controlled by comparison with ferrocene, added at the end of the measurement.

Luminescence titrations

dGMP titration experiment of complexes **3** were recorded on a Varian Cary Eclipse instrument. A solution of dGMP (5 mM) was progressively added to a solution of complex (50 µM) in 50 mM Tris-HCl buffer, pH = 7.4. Luminescence titration spectra with ODN (wtTel23 G-quadruplex DNA and HP-GC duplex DNA) were recorded in 10 mM HEPES, 35 mM NaCl, 50 mM KCl (pH=7.4) buffer on a Varian Cary Eclipse instrument. The titration was performed from the highest DNA concentration (10 µM) and progressively decreased it whereas the complex concentration (5 µM) was kept constant.

CD experiments

Prior to CD analysis, the oligonucleotides were annealed by heating the sample at 95°C for 5 min in buffer (10 mM Tris buffer pH 7.04) with 100 mM NaCl or KCl for wtTel23 and 100 mM NaCl for GC-AT hairpin, respectively, and cooling it overnight to room temperature. Analyses were recorded on a Jasco J-810 spectro-polarimeter using 1 cm length quartz cuvette. Spectra were recorded every 5°C, from 25°C to 90°C with a wavelength range from 220 to 330 nm. For each temperature, the spectrum

was an average of three scans with a 0.5 s response time, a 1 nm data pitch, a 4 nm bandwidth and a 200 nm min^{-1} scanning speed. For CD melting experiments, the ellipticity was recorded at 290 and 252 nm for wtTel23 and duplex hairpin, respectively. Melting temperatures were measured by using Boltzmann fitting on Origin software. Each curve fit was only accepted with r>0.99.

Bio layer interferometry (BLI)

BLI sensors coated with streptavidin (SA sensors) were purchased from Forte Bio (PALL). Prior to use, they were immerged 10 minutes in buffer before functionalization to dissolve the sucrose layer. Then the sensors were dipped for 15 minutes in DNA containing solutions (biotinylated systems **A-C**) at 100 nM and rinsed in buffer solution (10 mM HEPES pH 7.4, 35 mM NaCl, 50 mM KCl and 0.5% v/v surfactant P_{20}) for 10 minutes. The functionalized sensors were next dipped in different iridium(III) complex solution at different concentrations (see Figure 3 and Figure S24) for 2 minutes interspersed by a rinsing step in the buffer solution during 4 minutes. Reference sensors without DNA immobilization were used to subtract the non-specific adsorption on the SA layer. The sensorgrams were fitted using a heterogeneous model (see Figure 3 and Figure S24). The reported values are the means of representative independent experiments, and the errors provided are standard deviations from the mean. Each experiment was repeated at least two times.

Quantification of 8-oxodG by LC-MS-MS

The samples containing 100 µM of complex with 10 nmol of ODN (wtTel23 or HP-GC) in 200 µL of 10 mM HEPES (pH=7.4), 35 mM NaCl, 50 mM KCl buffer were irradiated (or not) during 30 minutes with blue LED system. 8-oxodG was quantified by HPLC coupled through electrospray ionization to tandem mass spectrometry (HPLC-MS/MS) as detailed previously [34] subsequently to enzymatic digestion of oligonucleotides.

ASSOCIATE CONTENT

Copies of NMR and MS spectra, absorption and luminescence spectra, cyclic voltammograms, CD, BLI and SPR sensorgrams.

AUTHOR INFORMATION

Corresponding Authors

* Benjamin.Elias@uclouvain.be

* Eric.Defrancq@univ-grenoble-alpes.fr

ORCID

Justin Weynand: /0000-0003-2104-7601

Frédérique Loiseau: /0000-0003-3648-4863

Jean-Luc Ravanat: /0000-0002-7123-6358

Jérôme Dejeu: /0000-0002-2434-2959

Eric Defrancq: /0000-0002-3911-6241

Benjamin Elias: /0000-0001-5037-3313

Notes

The authors declare no competing financial interest.

Acknowledgements

This work was supported by the *Fonds de la Recherche Scientifique – FNRS under Grant n°J.0091.18*. J.W. thanks the "Fonds pour la Formation à la Recherche dans l'Industrie et dans l'Agriculture" (F.R.I.A.) and the Erasmus programme for financial support. This work was partially supported by the "Agence National de la Recherche" (ANR-16-CE11-0006-01), Labex ARCANE and CBH-EUR-GS (ANR-17-EURE-0003) and the région Auvergne-Rhône-Alpes. The NanoBio-ICMG platforms (FR 2607) are acknowledged for their support. We also thank Dr L. Bonnat and Dr T. Lavergne for

providing bio-molecular systems **A**-**C**.

Entry for the Table of Contents (Please choose one layout)

Layout 1:

FULL PAPER

G-rich DNA targeting Ir(III) complexes: Three new photo-oxidizing iridium(III) complexes based on the 2-(4-chlorophenyl)-1H-imidazo[4,5-f][1,10]phenanthroline (CPIP) ligand have been synthesized. These complexes can photo-induced electron transfer with G-rich DNA structures.

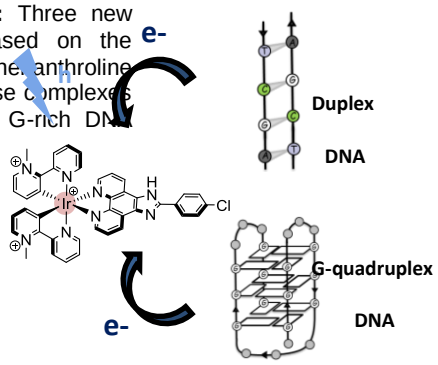

Justin Weynand, Hughes Bonnet, Frédérique Loiseau, Jean-Luc Ravanat, Jérôme Dejeu, Eric Defrancq, and Benjamin Elias**

Page No. – Page No.
Targeting G-rich DNA Structures with Photo-Reactive bis-Cyclometalated Iridium(III) Complexes

Keywords: G-quadruplex, photo-electron transfer, iridium complexes, DNA structures

References

[1] S. Neidle, S. Balasubramanian, *Quadruplex Nucleic Acids*, RSC Biomolecular Sciences, Cambridge, **2006**.

[2] V. S. Chambers, G. Marsico, J. M. Boutell, M. Di Antonio, G. P. Smith, S. Balasubramanian, *Nat. Biotechnol.* **2015**, *33*, 877.

[3] A. Bedrat, L. Lacroix, J.-L. Mergny, *Nucleic Acids Res*. **2016**, *44*, 1746.

[4] D. Rhodes, H. J. Lipps, *Nucleic Acids Res.* **2015**, *43*, 8627–8637.

[5] M. Métifiot, S. Amrane, S. Litvak, M.-L. Andreola, *Nucleic Acids Res.* **2014**, *42*,12352–12366.

[6] K. Paeschke, T. Simonsson, J. Postberg, D. Rhodes, H. J. Lipps, *Nature Structural & Molecular Biology* **2005**, *12*, 847-854.

[7] 7. R. J. O'Sullivan, J. Karlseder, *Nat Rev Mol Cell Biol.* **2010**, *11*, 171-181.

[8] N. Grandin, M. Charbonneau, *Biochimie* **2008**, 90, 41-59.

[9] 9. S. Victorelli, J. F. Passos, *EBioMedicine* **2017**, *21*, 14-20.

[10] D. Hanahan, R. A. Weinberg, *Cell* **2011**, *144*, 646–674.

[11] A. J. Cesare, R. R. Reddel, *Nat. Rev. Genet.* **2010**, *11*, 319–330.

[12] a) H. Han, L. H. Hurley, *Trends Pharmacol. Sci.* **2000**, *21*, 136–142; b) D. Monchaud, M-P. Teulade-Fichou, *Org. Biomol. Chem.* **2008**, *6*, 627–636; c) I. M. Dixon, F. Lopez, A. M. Tejera, J-P. Estève, M. A. Blasco, G. Pratviel, B. Meunier, *J. Am. Chem. Soc.* **2007**, *129*, 1502-1503; d) E. M. Rezler, J. Seenisamy, S. Bashyam, M-Y. Kim, E. White, W. D. Wilson, L. H. Hurley, *J. Am. Chem. Soc.* **2005**, *127*, 9439-9447.

[13] a) Q. Cao, Y. Li, E. Freisinger, P. Z. Qin, R. K. O. Sigel, Z-W. Mao, *Inorg. Chem. Front.* **2017**, *4*, 10-32; b) S. N. Georgiades, N. H. Abd Karim, K. Suntharalingam, R. Vilar, *Angew. Chem. Int. Ed.* **2010**, *49*, 4020-4034.

[14] S. Neidle, *Nat. Rev. Chem*. **2017**, 1, 0041.

[15] a) T-C. Liao, T-Z. Ma, Z. Liang, X-T. Zhang, C-Y. Luo, L. Liu, C-Q. Zhou, *Chem. Eur. J.* **2018**, *24*, 15840-

15851; b) C. Q. Zhou, T. C. Liao, Z. Q. Li, J. Gonzalez-Garcia, M. Reynolds, M. Zou, R. Vilar, *Chem. Eur. J.* **2017**, *23*, 4713–4722; c) A. Ali, M. Kamra, S. Roy, K. Muniyappa, S. Bhattacharya, *Bioconjugate Chem.* **2017**, *28*, 341–352.

[16] a) R. Kieltyka, P. Englebienne, J. Fakhoury, C. Autexier, N. Moitessier, H.F. Sleiman, *J. Am. Chem. Soc.* **2008**, *130*, 10040–10041; b) K. J. Castor, Z. Liu, J. Fakhoury, M. A. Hancock, A. Mittermaier, N. Moitessier, H. F. Sleiman, *Chem. Eur. J.* **2013**, *19*, 17836–17845.

[17] a) E. Wachter, D. Moyá, S. Parkin, E. C. Glazer, *Chem. Eur. J.* **2016**, *22*, 550-559; b) G. Piraux, L. Bar, M. Abraham, T. Lavergne, H. Jamet, J. Dejeu, L. Marcélis, E. Defrancq, B. Elias, *Chem. Eur. J.* **2017**, *23*, 11872–11880; c) L. Xu, X. Chen, J. Wu, J. Wang, L. Ji, H. Chao, *Chem. Eur. J.* **2015**, *21*, 4008–4020; d) X. Wang, L. Pei, X. Fan, S. Shi, *Inorg. Chem. Commun.* **2016**, *72*, 7–12.

[18] a) S. A. Archer, A. Raza, F. Dröge, C. Robertson, A. J. Auty, D. Chekulaev, J. A. Weinstein, T. Keane, A. J. H. M. Meijer, J. W. Haycock, S. MacNeil, J. A. Thomas. *Chem. Sci.* **2019**, *10*, 3502-3513; b) J. Weynand, A. Diman, M. Abraham, L. Marcélis, H. Jamet, A. Decottignies, J. Dejeu, E. Defrancq, B. Elias, *Chem. Eur. J.* **2018**, *24*, 15205-15210.

[19] D. Xia, B. Wang, B. Chen, S. Wang, B. Zhang, J. Ding, L. Wang, X. Jing, F. Wang, *Angew. Chem. Int. Ed.* **2014**, *53*, 1048-1052.

[20] a) C. Lentz, O. Schott, T. Auvray, G. Hanan, B. Elias, *Inorg. Chem.* **2017**, *56*, 10875-10881; b) A. Jacques, O. Schott, K. Robeyns, G. Hanan, B. Elias, *Eur. J. Inorg. Chem.* **2016**, 1779-1783.

[21] a) L. Lu, W. Wang, C. Yang, T-S. Kang, C-H. Leung, D-L. Ma, *J. Mater. Chem. B.* **2016**, *4*, 6791-6796; b) S. Lin, W. Wang, C. Hu, G. Yang, C-N. Ko, K. Ren, C-H. Leung, D-L. Ma, *J. Mater. Chem. B.* **2017**, *5*, 479-484; c) S. Lin, L. Lu, T-S. Kang, J-L. Mergny, C-H. Leung, D-L. Ma, *Anal. Chem.* **2016**, *88*, 10290-10295; d) L. Lu, M. Wang, Z. Mao, T-S. Kang, X-P. Chen, J-J. Lu, C-H. Leung, D-L. Ma, *Scientific Reports.* **2016**, *6*, 22458.

[22] K. J. Castor, K. L. Metera, U. M. Tefashe, C. J. Serpell, J. Mauzeroll, H. F. Sleiman, *Inorg. Chem.* **2015**, *54*,

6958–6967.

[23] a) A. Jacques, A. Kirsch-De Mesmaeker, B. Elias, *Inorg. Chem.* **2015**, *54*, 6958–6967; b) R. Bevernaegie, L. Marcélis, B. Laramée-Milette, J. De Winter, K. Robeyns, P. Gerbaux, G. S. Hanan, B. Elias, *Inorg. Chem.* **2018**, *57*, 1356-1367.

[24] K. Laws, A. Eskandari, C. Lu, K. Suntharalingam, *Chem. Eur. J.* **2018**, 24, 15205-15210.

[25] a) B. J. Coe, M. Helliwell, S. Sanchez, M.K. Peers, N. S. Scrutton, *Dalton Trans*. **2015**, *44*, 15420-15423; b) B. J. Coe, M. Helliwell, J. Raftery, S. Sanchez, M.K. Peers, N. S. Scrutton, *Dalton Trans*. **2015**, *44*, 20392-20405.

[26] P. Murat, Y. Singh, E. Defrancq, *Chem.Soc. Rev.* **2011**, *40*, 5293–5307.

[27] a) P. Murat, D. Cressend, N. Spinelli, A. Van der Heyden, P. Labbé, P. Dumy, E. Defrancq, *ChemBioChem*, **2008**, *9*, 2588-2591; b) P. Murat, R. Bonnet, A. Vander Heyden, N. Spinelli, P. Labbé, D. Monchaud, M.-P. Teulade-Fichou, P. Dumy, E. Defrancq, *Chem. Eur. J.* **2010**, *16*, 6106–6114; c) R. Bonnet, T. Lavergne, B. Gennaro, N. Spinelli, E. Defrancq, *Chem. Commun.* **2015**, *51*, 4850–4853.

[28] L. Bonnat, J. Dejeu, H. Bonnet, B. Génnaro, O. Jarjayes, F. Thomas, T. Lavergne, E. Defrancq, *Chem. Eur. J.* **2016**, *22*, 3139–3147.

[29] a) D. B. Hall, R. E. Holmlin, J. K. Barton, *Nature* **1996**, *382*, 731-735. b) C. J. Burrows, J. G. Muller, *Chem. Rev.* **1998**, 98, 1109-1151. c) J.-L. Ravanat, C. Saint-Pierre, J. Cadet, *J. Am. Chem. Soc*. **2003**, *125*, 2030-2031. d) T. Lindahl, *Nature*, **1993**, *362*, 709-715.

[30] S. Bielskutė, J. Plavec, P. Podbevšek, *J. Am. Chem. Soc.* **2019**, *141*, 2594-2603.

[31] G. Sathyaraj, M. Kiruthika, T. Weyhermüller, B. Unni Nair, *Dalton Trans.* **2012**, 41, 8460-8471.

[32] S. Sprouse, K.A. King, P.J. Spellane, R.J. Watts, *J. Am. Chem. Soc.* **1984**, 106, 6647-6653.

[33] A.M. Brouwer, *Pure Appl. Chem.* **2011**, 83, 2213-2228.

[34] J-L. Ravanat, T. Douki, P. Duez, E. Gremaud, K. Herbert, T. Hofer, L. Lasserre, C. Saint-Pierre, A. Favier, J. Cadet, *Carcinogenesis.* **2002**, 23, 1911-1918.